

# Numerical assessment of bone remodeling around conventionally and early loaded titanium and titanium–zirconium alloy dental implants

Kıvanç Akça · Atılım Eser · Yeliz Çavuşoğlu ·  
Elçin Sağırkaya · Murat Cavit Çehreli

Received: 19 June 2014 / Accepted: 18 February 2015 / Published online: 1 March 2015  
© International Federation for Medical and Biological Engineering 2015

**Abstract** The aim of this study was to investigate conventionally and early loaded titanium and titanium–zirconium alloy implants by three-dimensional finite element stress analysis. Three-dimensional model of a dental implant was created and a thread area was established as a region of interest in trabecular bone to study a localized part of the global model with a refined mesh. The peri-implant tissues around conventionally loaded (model 1) and early loaded (model 2) implants were implemented and were used to explore principal stresses, displacement values, and equivalent strains in the peri-implant region of titanium and titanium–zirconium implants under static load of 300 N with or without 30° inclination applied on top of the abutment surface. Under axial loading, principal stresses in both models were comparable for both implants and models. Under oblique loading, principal stresses around titanium–zirconium implants were slightly higher in both

models. Comparable stress magnitudes were observed in both models. The displacement values and equivalent strain amplitudes around both implants and models were similar. Peri-implant bone around titanium and titanium–zirconium implants experiences similar stress magnitudes coupled with intraosseous implant displacement values under conventional loading and early loading simulations. Titanium–zirconium implants have biomechanical outcome comparable to conventional titanium implants under conventional loading and early loading.

**Keywords** Early dental implant loading · Titanium · Titanium–zirconium alloy · Dental implant · Finite element stress analysis

## 1 Introduction

Osseointegration has been defined as the presence of structural and functional bone around a load-carrying implant [8]. This direct, ankylotic relationship between bone and implant without intervening connective or fibrous tissue could be confirmed at the light microscopy and ultrastructural levels [24, 29]. Osseointegrated dental implants are widely used for the rehabilitation of edentulous patients with predictably high success rates in the event certain preconditions, such as a suitable host, biocompatible material, optimum primary stability, careful implant surgery following a specific and strict protocol, and an appropriate interface healing time, are fulfilled [4]. Of these, loading protocols for implants have been amended to meet clinical expectations toward shortening the edentulous period [37]. Accordingly, early loading of titanium rough-surfaced dental implants placed without advanced surgical approaches has become a clinical routine. Apart from

---

K. Akça (✉)  
Department of Prosthodontics, Faculty of Dentistry, Hacettepe University, 06100 Sıhhiye, Ankara, Turkey  
e-mail: akcak@hacettepe.edu.tr; kivanc.akca@superonline.com

A. Eser  
Institute for Materials Applications in Mechanical Engineering, RWTH Aachen University, Aachen, Germany

Y. Çavuşoğlu  
Section of Prosthodontics, Acıbadem Ataşehir Medical Surgery Center, Ataşehir, Istanbul, Turkey

E. Sağırkaya  
Department of Prosthodontics, Faculty of Dentistry, Ordu University, 52200 Ordu, Turkey

M. C. Çehreli  
Section of Prosthodontics, CosmORAL Oral and Dental Health Polyclinics, Cinnah Str. 7/5, 06680 Kavaklıdere, Ankara, Turkey

advances in loading protocols, the strength of conventional titanium implant material has been altered by conversion into a novel titanium–zirconium (TiZr) alloy lately, originally to improve the fatigue performance of narrow-diameter implants. The idea behind this approach is to have narrow-diameter implants presenting similar mechanical properties with standard diameter titanium implants toward critical treatment planning. With this, it is assumed to have less advanced surgical techniques to shorten healing time and decrease risk of biologic complications as well. The high-strength TiZr alloy consists of more than 99.6 % titanium and zirconium, mainly in a monophasic  $\alpha$ -structure, with up to 10 %  $\alpha/\beta$  permitted in the raw material and has Young's modulus slightly lower than titanium [6]. While the TiZr alloy implant has showed higher removal torque values in an animal study [16], the information regarding bone-to-implant contact seems inconclusive so far [16, 32]. Therefore, appropriate timing for the functional loading of TiZr implants remains unclear. Nevertheless, the short-term effectiveness (up to 24 months) of conventionally, immediately, and early-loaded TiZr alloy narrow-diameter implants shows favorable biologic outcome [2, 6, 10].

As a living material, bone is uniquely capable of responding and adapting to mechanical cues that influence its size and shape [15, 21]. Therefore, defining the mechanical environment around peri-implant tissues for different loading protocols and/or implant materials is a gateway to better understanding the mechanisms of osseointegration [35]. Owing to demanding nature of animal studies, numerical simulations have been employed to investigate the biomechanics of orthopedic and dental implants. Moreover, analysis based on computational simulations are more capable to reveal additional information compared to on-site testing with localized predetermined conditions such as with strain gauges [9]. Individualized finite element modeling with or without automatic mesh generation [34, 36] and implementation of animal/human stress/strain

or histomorphometric data [5, 12, 25, 35] have been used to optimize the resolution and numerical accuracy of finite element analyses. So far, the time-dependent biomechanics of titanium implants under different loading conditions has been investigated by numerical analysis [5, 12, 38]. Recently, peri-implant bone remodeling around TiZr alloy implants with different designs has been evaluated with time-dependent finite element analyses [13]. The information has yet to be expanded for better understanding of biomechanical behavior of TiZr alloy implants. Therefore, the purpose of this study was to investigate conventionally and early loaded titanium and TiZr alloy implants by means of numerical analysis employed at a region of interest.

## 2 Materials and methods

Numerical models were generated to investigate the peri-implant mechanical events around conventionally loaded implants with 12 weeks of interface healing and early loaded implants after 4 weeks of interface healing. The loading simulations as well as the bone parameters were designed and modeled according to the histologic, histometric, and morphometric data around a rough-surfaced implant presented elsewhere [1, 5, 7].

### 2.1 Submodeling of a global model

The submodeling procedure described previously has been followed [3]. In brief, an implant thread with surrounding trabecular bone tissue was modeled with a refined mesh based on the solution from a global model of a soft tissue level dental implant dimensions with  $\text{Ø } 4.1 \times 12 \text{ mm}$  [Regular Neck Standard Plus (043.033S); Institut Straumann, Basel, Switzerland) and its solid abutment (048.541; Institut Straumann)] with a coarse mesh, where node-based technique was applied (Fig. 1). Macro-geometry of the

**Fig. 1** Modeled dental implant

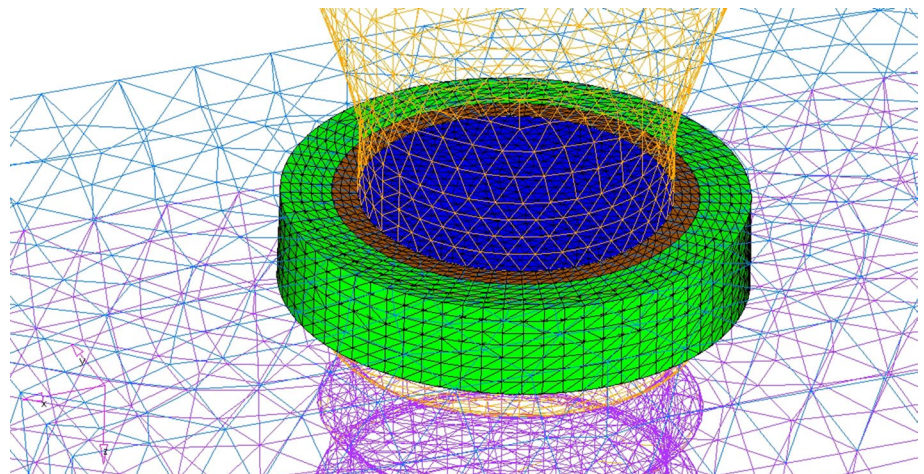


**Fig. 2** Peri-implant area of model 1. ROI: Elements in *yellow color* represent bone marrow; n-ROI and a-ROI: Elements in *light blue color* represent mature bone (color figure online)

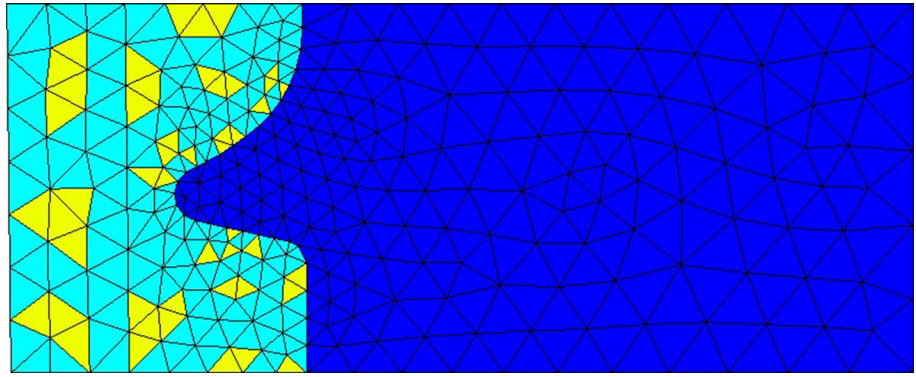
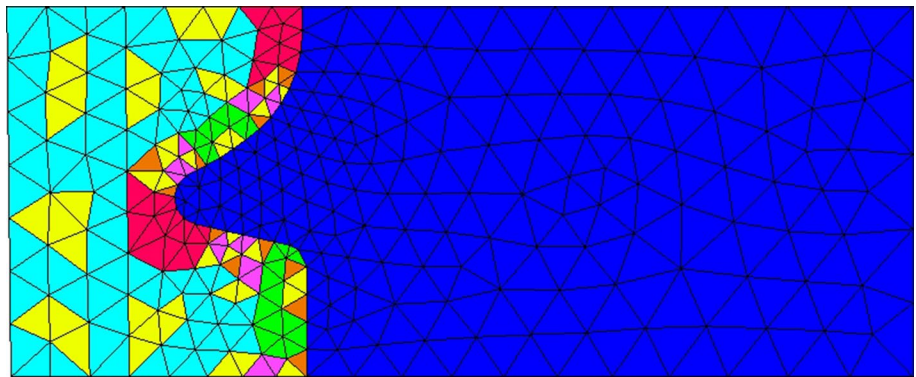


**Fig. 3** Peri-implant area of model 2. ROI: Elements in *yellow color* represent bone marrow; n-ROI: Elements in *light blue color* represent mature bone; a-ROI: Elements in *red color* represent mature bone, *green color* represent lamellar bone, *brown color* represent parallel fibered bone, and *purple color* represent woven bone (color figure online)



implant and integrated abutment surface design was created using a 3D CAD design software (Catia V5, 3DS Dassault Systèmes, Vélizy-Villacoublay, France) according to the disclosed dimensions on implant transmucosal neck/intraosseous body parts, thread pitch/angle, and abutment height/angle at product catalog and information documentations (Institut Straumann). The implant was aligned vertically in the center of a rectangular prism representing trabecular bone with 1-mm-thick cortical bone. The displacements were derived from the global analyses and used for the submodel analyses. Two submodels with refined meshes representing 12 weeks (model 1) and 4 weeks (model 2) interface healing were modeled for simulation of conventional and early loading conditions, respectively.

## 2.2 Peri-implant remodeling of bone

Two regions of interest (ROI) were defined referring to implant surface: adjacent (a-ROI) and near (n-ROI) in the peri-implant region. a-ROI was defined to simulate different states of bone–implant interface with a width of 0.25 mm adjacent to implant surface. The remaining area resting in 0.9-mm-wide peri-implant bone was assumed to be neighboring constant bone support (n-ROI). Generation of the trabecular bone and the element selection process for a-ROIs was based on histomorphometric data in the vicinity of implant thread. The procedure is explained in detail

elsewhere [3]. Mature bone was considered for the elements at the n-ROIs. Consequently, model 1 and model 2 were associated with different skeletal tissue components at the a-ROIs [7] (Figs. 2, 3).

## 2.3 Preprocessing, analyses, and postprocessing

Modeling and analysis/visualization procedures were carried out using MSC.Marc.Mentat 2003 (MSC Software Corporation, Los Angeles, CA, USA) and Abaqus 6.5.1-Abaqus/Viewer (Simulia, Providence, RI), respectively. The global model with a coarse mesh was created using 3D second-order tetrahedral elements (Abaqus Element Library: element type C3D10) with ten nodes, with 25,165 and 41,886 numbers, respectively. Element density was increased within a mesh convergence analysis, and the elements numbers mentioned found to be adequate for the simulations in this study. The element quality was verified for free of distortion using Abaqus standard element quality criteria. Then, a 2D finite element mesh generation was performed for the submodels following an approach described previously [3]. The material properties of the materials and tissues implemented are presented in Table 1. All materials were assumed to be homogenous, isotropic, and linearly elastic. Either contact or bond relationships were implemented between the elements in a-ROIs and the implant surface, based on the peri-implant healing

state. 3D finite element model conversions were undertaken by 360° axial rotation of the planar models followed by visualization and verification of the 3D submodels with second-order triangular prism and brick elements (Abaqus Element Library: element type C3D15 and C3D20). An element quality check was applied to the global model and the submodels, and no distorted element was detected. The implants and their loading status were analyzed under static load of 300 N with or without 30° inclination applied on top of the abutment surface, where submodel analyses were run separately. The boundary conditions for the global model were established by fixing the entire rectangular bone prism in all degrees of freedom in -x, -y, and -z directions and were set far enough from the region of interest, according to Saint-Venant's principle [33] to minimize its effect at the bone–implant interface. Submodels used the displacements from the global analysis as a boundary

load seed. Maximum and minimum principal stresses, total displacement, and equivalent total strain developed at the elements in the a-ROIs were recorded separately to calculate the mean for each bone type at mid-planar section. In addition, the highest values at a-ROIs were calculated. Apart from output scalars, distribution characteristics in the n-ROIs were also evaluated visually.

### 3 Results

#### 3.1 Quantification of outputs at a-ROIs

Under axial loading, the minimum and maximum principal stresses in model 1 and model 2 were similar for both Ti and TiZr implants. The mean minimum and maximum principal stresses in model 1 and model 2 were similar, and the highest maximum principal stresses in model 2 were slightly higher than those of model 1 (Table 2). Oblique loading resulted in higher stress fields around both type of implants in both models. Under oblique loading, the minimum and maximum principal stresses around TiZr implants were slightly higher than those around Ti implants in model 1 and model 2. Comparable stress magnitudes were observed for model 1 and model 2, although mean maximum principal stresses were slightly higher in model 2 (Table 3). The mean and highest total displacement values for Ti and TiZr implants were similar in model 1 and model 2. The mean total displacement values for TiZr implants were lower than those for Ti implants in model 1 under axial and oblique loading, although displacement values for the implants studied were below 1 μm. The mean and highest total displacement values in model 2 were similar for both Ti and TiZr implants and also to model 1 values. Equivalent strains around TiZr implants were

**Table 1** Material properties utilized in the analyses

Material	Young's modulus (GPa)	Poisson's ratio	References
Cortical bone/mature	22.5	0.3	[26]
Trabecular bone/woven	2.11	0.3	[28]
Trabecular bone/parallel fibered	3.8	0.3	[20]
Trabecular bone/lamellar	6.6	0.3	[22]
Trabecular bone/mature	13.4	0.3	[26]
Commercially pure titanium	114	0.369	[23]
Titanium–zirconium alloy	100	0.3	[18]

**Table 2** Minimum and maximum principal stresses around model 1 and model 2 under axial loading

Model 1						Model 2					
Light blue trabecular		Red trabecular		Green trabecular		Brown trabecular		Purple trabecular		Light blue trabecular	
Mean	Highest	Mean	Highest	Mean	Highest	Mean	Highest	Mean	Highest	Mean	Highest
<i>Minimum principal stress</i>											
Ti–Zr											
-5.13	-17.98	-4.92	-13.28	-1.62	-6.08	-1.20	-3.06	-1.01	-3.66	-4.76	-17.75
Ti											
-4.99	-17.65	-4.84	-13.18	-1.53	-5.91	-1.10	-2.95	-0.92	-3.48	-4.59	-17.64
<i>Maximum principal stress</i>											
Ti–Zr											
3.54	15.61	3.68	12.42	2.07	12.12	1.15	5.46	0.80	5.53	3.41	17.45
Ti											
3.57	15.65	3.75	12.51	2.11	12.33	1.20	5.81	0.84	5.79	3.45	17.54

**Table 3** Minimum and maximum principal stresses around model 1 and model 2 under oblique loading

Model 1										Model 2	
Light blue trabecular		Red trabecular		Green trabecular		Brown trabecular		Purple trabecular		Light blue trabecular	
Mean	Highest	Mean	Highest	Mean	Highest	Mean	Highest	Mean	Highest	Mean	Highest
<i>Minimum principal stress</i>											
Ti–Zr											
-8.23	-57.31	-7.83	-33.18	-3.26	-19.98	-2.53	-13.06	-1.99	-16.40	-8.18	-57.18
Ti											
-7.83	-55.63	-7.49	-33.14	-2.99	-19.03	-2.31	-12.37	-1.80	-15.40	-7.71	-55.50
<i>Maximum principal stress</i>											
Ti–Zr											
6.35	28.55	6.42	26.93	3.71	17.59	2.45	13.77	1.81	11.19	6.69	28.89
Ti											
6.09	27.45	6.17	25.53	3.58	16.95	2.36	12.81	1.75	10.55	6.40	27.80

**Table 4** Total displacement and equivalent total strain in model 1 and model 2 under axial loading

Model 1										Model 2	
Light blue trabecular		Red trabecular		Green trabecular		Brown trabecular		Purple trabecular		Light blue trabecular	
Mean	Highest	Mean	Highest	Mean	Highest	Mean	Highest	Mean	Highest	Mean	Highest
<i>Total displacement</i>											
Ti–Zr											
0.00614	0.00898	0.00452	0.00903	0.00399	0.00890	0.00399	0.00898	0.00393	0.00896	0.00700	0.00903
Ti											
0.00846	0.00891	0.00865	0.00895	0.00867	0.00884	0.00866	0.00890	0.00865	0.00889	0.00853	0.00895
<i>Equivalent total strain</i>											
Ti–Zr											
0.00050	0.00130	0.00050	0.00105	0.00043	0.00112	0.00050	0.00105	0.00070	0.00162	0.00047	0.00133
Ti											
0.00049	0.00128	0.00049	0.00109	0.00049	0.00107	0.00068	0.00159	0.00043	0.00112	0.00046	0.00131

comparable to Ti implants in both models under axial loading and oblique loading (Tables 4, 5).

### 3.2 Qualification outputs at n-ROIs

Stress, displacement, and strain distribution in model 1 and model 2 were indistinguishable for both Ti and TiZr implants under both loading conditions. Under axial and oblique loading conditions, displacement contour plots display identical bone deformation for both models and implant types (Figs. 4, 5).

## 4 Discussion

The Young’s modulus of the implant material has long been a topic of research interest in the field of orthopedics and

dentistry. As the elastic modulus of the implant and the bone are different, stress transfer between an implant and surrounding bone is not homogeneous. This phenomenon, defined as stress shielding, might reduce the stimulation of peri-implant bone tissue and could explain bone atrophy and sometimes loosening of hip implants and fracture of the bone [19]. Concerning dental implants, there has not been any published evidence of implant failure caused by stress shielding, although studies on the consequences of Young’s modulus have been undertaken by numeric analyses. While Rieger et al. [27] recommended the use of tapered dental implants with a high Young’s modulus, Hedia [17] reported that reduction in the Young’s modulus of the implant could reduce the stresses in the cortical and trabecular bone by 16 and 15 %, respectively. In an animal and numerical validation study, Stoppie et al. [30] found that a titanium-coated high-density polyethylene implant

**Table 5** Total displacement and equivalent total strain in model 1 and model 2 under oblique loading

Model 1										Model 2	
Light blue trabecular		Red trabecular		Green trabecular		Brown trabecular		Purple trabecular		Light blue trabecular	
Mean	Highest	Mean	Highest	Mean	Highest	Mean	Highest	Mean	Highest	Mean	Highest
<i>Total displacement</i>											
Ti–Zr											
0.00588	0.01637	0.00436	0.01592	0.00368	0.01524	0.00372	0.01530	0.00366	0.01530	0.00664	0.01637
Ti											
0.00806	0.01606	0.00837	0.01563	0.00802	0.01499	0.00811	0.01504	0.00810	0.01504	0.00813	0.01606
<i>Equivalent total strain</i>											
Ti–Zr											
0.00086	0.00342	0.00084	0.00230	0.00084	0.00242	0.00110	0.00260	0.00152	0.00421	0.00089	0.00344
Ti											
0.00082	0.00332	0.00081	0.00229	0.00079	0.00230	0.00103	0.00242	0.00142	0.00396	0.00084	0.00333

with low Young's modulus (1 GPa) had higher bone mass in the peri-implant zone after 6 months of loading than titanium implants, which was attributed to anabolic strains experienced in peri-implant bone. In the present study, the Young's modulus of the TiZr alloy implant (100 GPa) was slightly lower than the titanium implant (110 GPa), and this resulted in a stress field comparable to conventional titanium implants. While the effect of this difference was not observed during axial loading, where comparable stresses were recorded, the slightly higher compressive and tensile stresses observed in the periphery of TiZr alloy implants under conventional and early loading might be related to relatively lower Young's modulus of this alloy. It is unknown whether the slight increase in stresses under oblique loading would lead to anabolic effects and increase in bone mass around the periphery of TiZr implants, as histomorphometric bone-to-implant measurements for conventionally and early loaded TiZr implants has not been undertaken so far. Concerning the unloaded state, however, both types of implants show comparable outcomes. Four-week histomorphometric bone-to-implant contact results of one study showed comparable outcomes for TiZr and titanium implants [16], whereas a statistically insignificant slight delay was observed for TiZr implants in another animal study [32]. Eser et al. [13] presented similar peri-implant bone remodeling properties around TiZr implant under immediate loading conditions in comparison with Ti implants using computer simulation based on a time-dependent algorithm. Overall comparably, the outcomes of the current study suggest that peri-implant stresses and equivalent strain amplitudes particularly at the vicinity of TiZr implants experienced under axial and oblique loading are similar to Ti implants under conventional loading and early loading at the focused area. Therefore, in

interpretation of this outcome for clinical practice, evidence-based loading protocols for titanium dental implants may be applicable to novel titanium–zirconium alloyed dental implants [14].

The amount of axial/lateral displacement of a loaded implant can be influenced by several factors such as its design and the density of host bone. At the experimental level, this displacement can be measured directly by displacement sensors or may be predicted means of numeric analysis. The critical threshold of displacement above which fibrous encapsulation and failure of the implant occurs is probably above 150  $\mu\text{m}$  [31], as generally interpreted, although there is not any sound evidence in the context of dental implants. In the present study, the only difference detected in displacement values was that mean displacement values of TiZr implants were lower than those for Ti implants in model 1 under axial and oblique loading. Considering that other displacement values were very close and all values were below 1  $\mu\text{m}$ , the biologic effect of this difference would be negligible under conventional loading and early loading. In addition, considering the Young's modulus of the implants tested, the outcome will also be negligible, as Stoppie et al. [30] could not establish any correlation with relative micromotion and tissue response to loaded titanium-coated high-density polyethylene implants with low Young's modulus (1 GPa) or titanium implants. Thus, bone deformation findings around TiZr implants suggest that the overall stiffness of implant–bone complex may represent similar intraosseous implant stability behavior for titanium implants [11]. From this aspect, biomechanical stability of novel titanium–zirconium alloyed implants is clinically acceptable for functional loading conditions.

Due to increasing difficulties in experimental study designs both preclinical and clinical, use of in silico

**Fig. 4** Displacements at parallel sides in model 1 for titanium implant (a and b) and for titanium–zirconium alloy implant (c and d) under axial loading. Displacements at parallel sides in model 2 for titanium implant (e and f) and for titanium–zirconium alloy implant (g and h) under axial loading

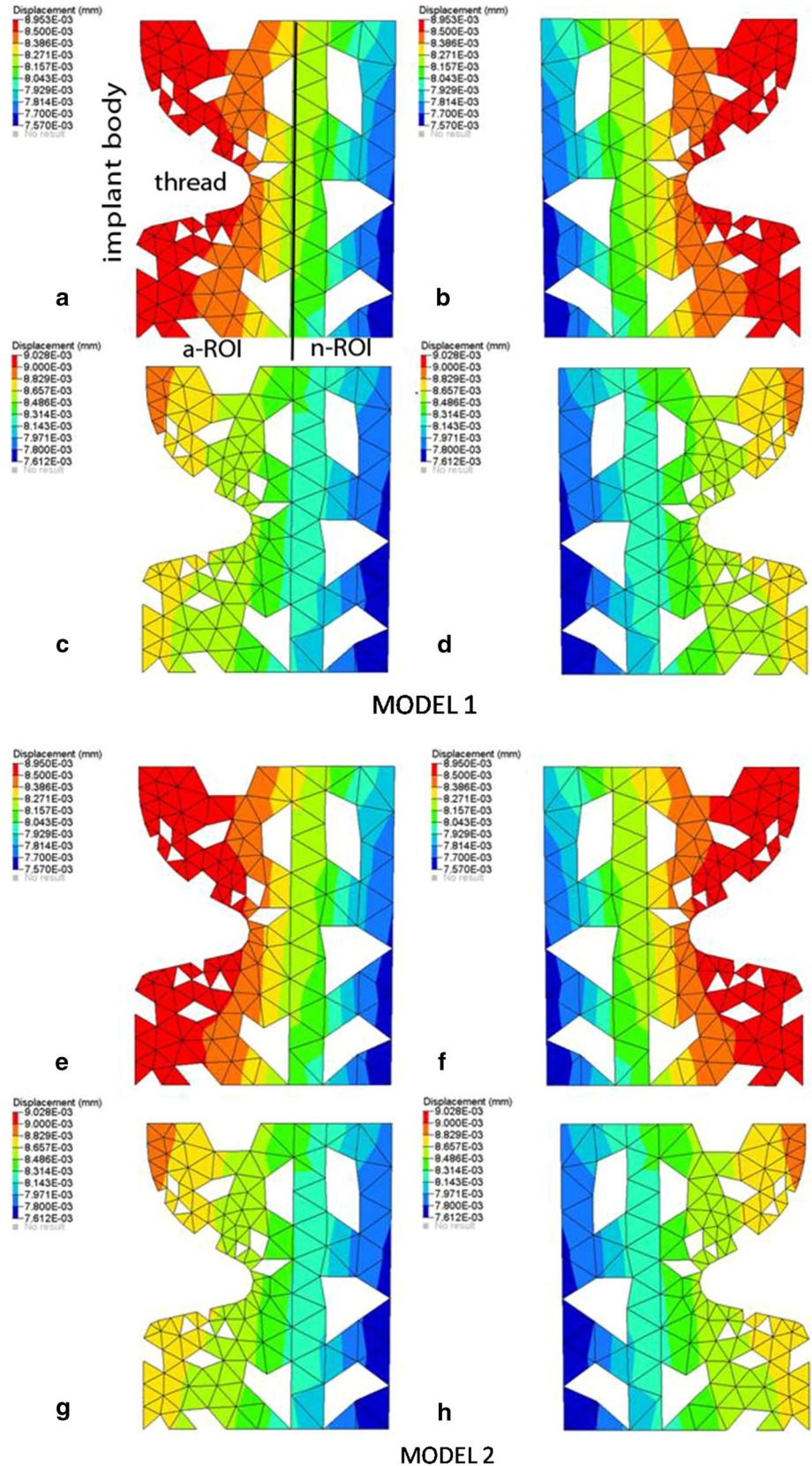
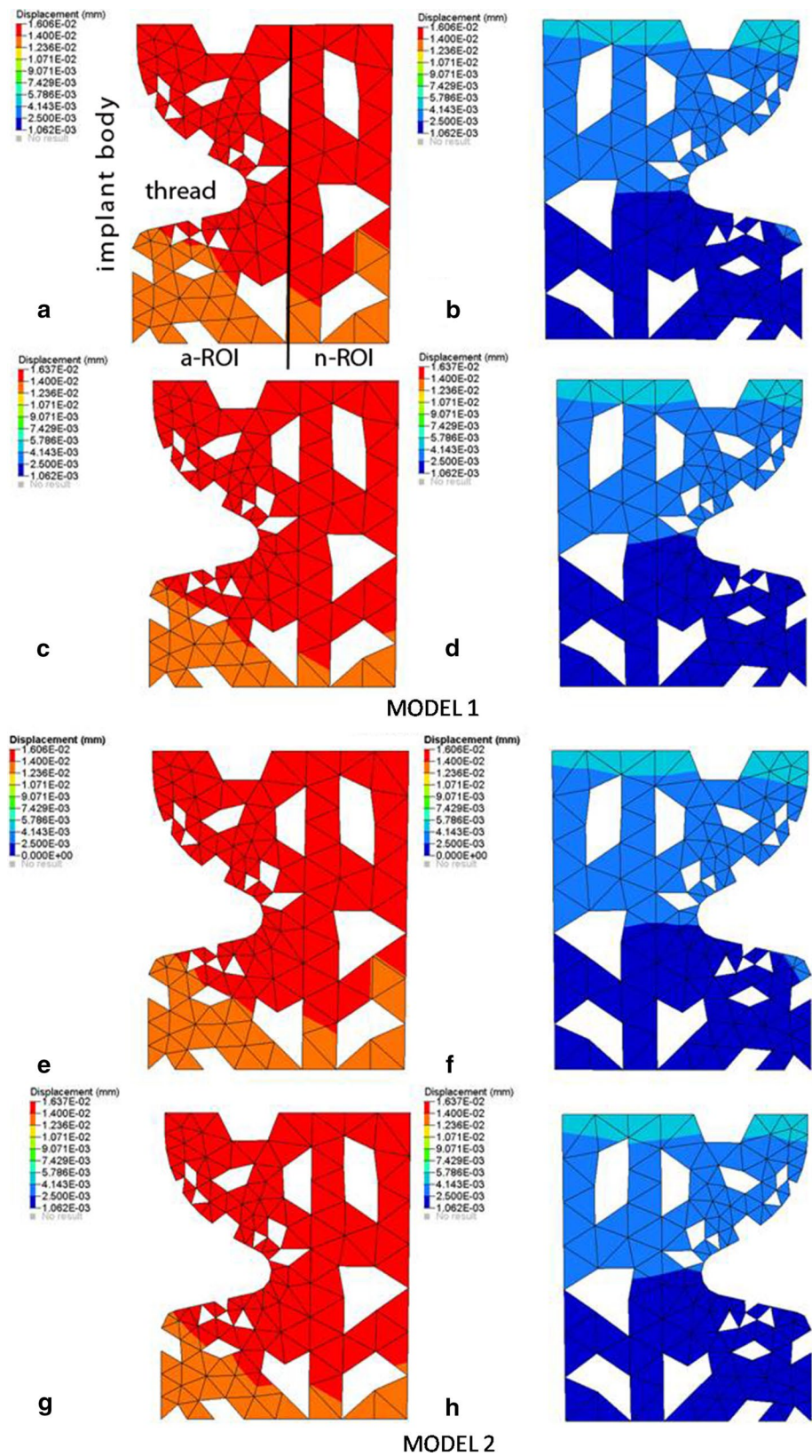


**Fig. 5** Displacements in model 1 for titanium implant under oblique loading at compression (a) and tension sides (b) and for titanium–zirconium alloy implant at compression (c) and tension sides (d). Displacements in model 2 for titanium implant under oblique loading at compression (e) and tension sides (f) and for titanium–zirconium alloy implant at compression (g) and tension sides (h). Tension side: side of load application, compression side: the opposite side of load application





approaches has a potential to premise recommendations on practices. However, the data obtained under such conditions should always be concerned with regard to complexity of living systems. Therefore, outcomes from studies lacking in internal and/or external verification should be followed cautiously for correct clinical interpretations.

## 5 Conclusion

Within the confines of this study, it is predicted that implant material (conventional titanium vs. titanium–zirconium alloy) and the loading state (conventional loading vs. early loading) leads to comparable biomechanical outcomes. The new titanium–zirconium alloy with higher mechanical strength and relatively lower Young's modulus might show similar stress/strain fields and intraosseous displacement values like conventional titanium implants under both conventional loading and early loading conditions.

## References

1. Abrahamsson I, Berglundh T, Linder E et al (2004) Early bone formation adjacent to rough and turned endosseous implant surfaces. An experimental study in the dog. *Clin Oral Implants Res* 15:381–392
2. Akca K, Cavusoglu Y, Uysal S et al (2013) A prospective, open-ended, single-cohort clinical trial on early loaded Titanium–zirconia alloy implants in partially edentulous patients: up-to-24-month results. *Int J Oral Maxillofac Implants* 28:573–578
3. Akca K, Eser A, Canay S (2010) Numerical simulation of the effect of time-to-loading on peri-implant bone. *Med Eng Phys* 32:7–13
4. Albrektsson T, Brånemark P-I, Hasson HA et al (1981) Osseointegrated titanium implants. Requirements for ensuring a longlasting direct bone to implant anchorage in man. *Acta Orthop Scand* 52:155–170
5. Amor N, Geris L, Vander Sloten J et al (2009) Modelling the early phases of bone regeneration around an endosseous oral implant. *Comput Methods Biomech Biomed Eng* 12:459–468
6. Barter S, Stone P, Brägger U (2012) A pilot study to evaluate the success and survival rate of titanium–zirconium implants in partially edentulous patients: results after 24 months of follow-up. *Clin Oral Implants Res* 23:873–881
7. Berglundh T, Abrahamsson I, Lang NP et al (2003) Denovo alveolar bone formation adjacent to endosseous implants. A model study in the dog. *Clin Oral Impl Res* 14:251–262
8. Brånemark PI, Hansson BO, Adell R et al (1977) Osseointegrated implants in the treatment of the edentulous jaw. Experience from a 10-year period. *Scand J Plast Reconstr Surg* 16:1–132
9. Cehreli MC, Akkocaoglu M, Comert A et al (2007) Bone strains around apically free versus grafted implants in the posterior maxilla of human cadavers. *Med Biol Eng Comput* 45:395–402
10. Chiapasco M, Casentini P, Zaniboni M et al (2012) Titanium–zirconium alloy narrow-diameter implants (Straumann Roxolid®) for the rehabilitation of horizontally deficient edentulous ridges: prospective study on 18 consecutive patients. *Clin Oral Implants Res* 23:1136–1141
11. Dias DR, Leles CR, Lindh C et al (2014) The effect of marginal bone level changes on the stability of dental implants in a short-term evaluation. *Clin Oral Implants Res*. doi:10.1111/clr.12426
12. Eser A, Tonuk E, Akca K et al (2010) Predicting time-dependent remodeling of bone around immediately loaded dental implants with different designs. *Med Eng Phys* 32:22–31
13. Eser A, Tönük E, Akca K et al (2013) Predicting bone remodeling around tissue- and bone-level dental implants used in reduced bone width. *J Biomech* 46:2250–2257
14. Gallucci GO, Benic GI, Eckert SE et al (2014) Consensus statements and clinical recommendations for implant loading protocols. *Int J Oral Maxillofac Implants* 29(suppl):287–290
15. Giesen EB, Ding M, Dalstra M et al (2003) Reduced mechanical load decreases the density, stiffness, and strength of cancellous bone of the mandibular condyle. *Clin Biomech* 18:358–363
16. Gottlow J, Dard M, Kjellson F et al (2012) Evaluation of a new titanium–zirconium dental implant: a biomechanical and histological comparative study in the mini pig. *Clin Implant Dent Relat Res* 14:538–545
17. Hedia HS (2002) Stress and strain distribution behavior in the bone due to the effect of cancellous bone, dental implant material and the bone height. *Biomed Mater Eng* 12:111–119
18. Ho W-F, Chen W-K, Wu S-C et al (2008) Structure, mechanical properties, and grindability of dental Ti–Zr alloys. *J Mater Sci Mater Med* 19:3179–3186
19. Huijskes R, Weinans H, Grootenboer HJ et al (1987) Adaptive bone-remodeling theory applied to prosthetic-design analysis. *J Biomech* 20:1135–1150
20. Jensen KS, Mosekilde A (1990) A model of vertebral trabecular bone architecture and its mechanical properties. *Bone* 11:417–423
21. Jones HH, Priest JD, Hayes WC et al (1977) Humeral hypertrophy in response to exercise. *J Bone Jt Surg Am* 59:204–208
22. Ladd AJC, Kinney JH, Haupt DL et al (1998) Finite element modeling of trabecular bone: comparison with mechanical testing and determination of tissue modulus. *J Orthop Res* 16:622–628
23. Merz BR, Hunenbart S, Belsler UC (2000) Mechanics of the implant–abutment connection: an 8-degree taper compared to a butt joint connection. *Int J Oral Maxillofac Implants* 15:519–526
24. Meyer U, Joos U, Mythili J et al (2004) Ultrastructural characterization of the implant/bone interface of immediately loaded dental implants. *Biomaterials* 25:1959–1967
25. Moreo P, García-Aznar JM, Doblaré M (2008) Bone ingrowth on the surface of endosseous implants. Part 1. Mathematical model. *J Theor Biol* 260:1–12
26. Rho JY, Tsui TY, Pharr GM (1997) Elastic properties of human cortical and trabecular bone measured by nanoindentation. *Biomaterials* 18:1325–1330
27. Rieger MR, Fareed K, Adams WK et al (1986) Bone stress distribution for three endosseous implants. *J Prosthet Dent* 61:223–228
28. Riemer BA, Eadie JS, Wenzel TE, et al (1995) Microstructure and material property variations in compact and trabecular vertebral bone tissues. In: 41st Annual meeting of Orthopaedic Research Society, vol 2, p 529
29. Stefflik DE, McKinney RV Jr, Koth DL et al (1984) The biomaterial-tissue interface: a morphological study utilizing conventional and alternative ultrastructural modalities. *Scanning Electron Microsc Pt* 2:547–555
30. Stoppie N, Van Oosterwyck H, Jansen J et al (2009) The influence of Young's modulus of loaded implants on bone remodeling: an experimental and numerical study in the goat knee. *J Biomed Mater Res A* 90:792–803
31. Szmukler-Moncler S, Salama H, Reingewirtz Y et al (1998) Timing of loading and effect of micromotion on bone–dental implant interface: review of experimental literature. *J Biomed Mater Res* 43:192–203
32. Thoma DS, Jones AA, Dard M et al (2011) Tissue integration of a new titanium–zirconium dental implant: a comparative histologic and radiographic study in the canine. *J Periodontol* 82:1453–1461

33. Ugural AC, Fenster SK (2003) *Advanced strength and applied elasticity*, 4th edn. Pearson Education – Prentice Hall, Englewood Cliffs, NJ, p 83
34. van Rietbergen B, Weinans H, Huiskes R (1997) Prospects of computer models for the prediction of osteoporotic bone fracture risk. In: Lowet G, Rüesgsegger P, Weinans H, Meunier A (eds) *Bone research in biomechanics*. IOS Press, Netherlands, pp 25–32
35. Vandamme K, Naert I, Duyck J (2012) Animal experimental findings on the effect of mechanical load on peri-implant tissue differentiation and adaptation. In: Cehreli M (ed) *Biomechanics of oral implants: handbook for researchers*. Nova Science, New York, pp 97–127
36. Viceconti M, Davinelli M, Taddei F et al (2004) Automatic generation of accurate subject-specific bone finite element models to be used in clinical studies. *J Biomech* 37:1597–1605
37. Weber HP, Morton D, Gallucci GO et al (2009) Consensus statements and recommended clinical procedures regarding loading protocols. *Int J Oral Maxillofac Implants* 24(suppl):180–183
38. Wintera W, Heckmann SM, Weber HP (2004) A time-dependent healing function for immediate loaded implants. *J Biomech* 37:1861–1867